Schedule for Presentation Meeting of Master-Degree Thesis in 2020
International Course of Maritime & Urban Engineering

Date :　　July 29th (Wednesday) starting from 09:30

Venue :　　S1-312 Lecture Room

No.	Time	Name	Supervisor	Title of thesis	Chairman
1	09:30 – 09:55	AHMED Murshalin	Sanada	FE Modelling of Reinforced Concrete Exterior Beam-Column Joint with Deficient Beam Longitudinal Reinforcement Anchorage	Matsubara
2	09:55 – 10:20	NER Nikko Torres	Kita	Flood Coping Mechanisms in In-city Resettlement Areas: A Case Study of Barangay Malanday in Marikina City, Philippines	Matsubara
3	10:20 – 10:45	RAHMAN Tahmina	Kita	A Study on the Potentials of Green Blue Infrastructure (GBI) Network for Dhaka City in Bangladesh	Matsubara
4	10:50 – 11:15	NALLARAJAH Renee Josiah	Araki	Impacts of Tsunami Driven Debris on Onshore Coastal Structures	Araki
5	11:15 – 11:40	BUERLIHAN Ayang	Tsutsumi	Study on the effect of weld bead shape on fatigue strength of Out-of-Plane Gusset	Araki
Lunch Break					
6	13:00 – 13:25	SUBRAMANIAM Sreenath	Umeda	Systematic Study of Water-on-Deck Effect of Offshore Supply Vessel Running in Stern Quartering Waves	Maki
7	13:25 – 13:50	ISNAINI Rodhiatul	Iijima	Still Water Bending Moment Evaluation on Beam through Cargo Loading Prediction using Kalman Filter	Maki
8	13:50 – 14:15	Thein Lin Aung	Ma	Development of Iso-Geometric Analysis Software JWRIAN-IGA for Weld Bead Geometry Design Using Bayesian Optimization	Maki
9	14:15 – 14:40	RACHMAN Dimas Maulana	Maki	Study of Automatic Berthing by Evolution Strategy with Covariance Matrix Adaptation (CMA-ES) in Real Time	Maki
	14:55 –	at S1-312　　Meeting for Evaluating Master-thesis Presentations, and Steering Committee Meeting				

Meeting for Evaluation:　　From 14:55 at S1-312 Lecture Room

　　　　　　　　　　　　　Members are Steering committee members and the supervisors

FE Modelling of Reinforced Concrete Exterior Beam-Column Joint with Deficient Beam Longitudinal Reinforcement Anchorage

Murshalin Ahmed

Concrete Structure Laboratory, Department of Architectural Engineering

Key Words: *Bond-slip, Deficient anchorage, Exterior joint, FEM analysis, Low strength concrete*

1. Introduction

The application of straight anchorage at the exterior beam-column joint is often found in developing countries because of the simplicity of its installation. In this study, nonlinear 2-D finite element analysis was conducted on reinforced concrete (RC) exterior beam-column joint specimen with deficient beam rebar anchorage and the seismic capacity was predicted. The results by the finite element analysis were also compared with the experimental results. The research describes the effectiveness of modeling of the straight anchorage considering the bond-slip relationship between the rebar and concrete and its limitations.

2. Finite Element Analysis

2.1 FE Modelling

The specimen analyzed was the specimen J1 from the previous study[1], as shown in **Fig. 1**. **Table 1** shows the specification of specimen J1. An image of analytical modeling is shown in **Fig. 2**. Concrete and pin supports were modeled by four-node isoparametric quadrilateral elements in 2-D discretization. Longitudinal bars in the beam and column were modeled by discrete truss elements to consider bond behavior between reinforcing bar and concrete. The bond behavior was modeled by introducing a linkage element on the interface between the truss element and the concrete element. All other reinforcing bars were modeled by embedded elements, assuming perfect bonding. The mechanical properties of concrete and reinforcements were referred to the experimental results, as shown in **Table 1**.

Table 1 Specification of the specimen

Column	b x D	270 mm x 270 mm
	Main rebar	10-D13
	Shear reinf.	D6@60
Beam	b x D	210 mm x 370 mm
	Main rebar	8-D13
	Shear reinf.	D6@60
Concrete compressive strength/Steel yield stress	Concrete	11.0 N/mm²
	D13	342 N/mm²
	D6	408 N/mm²
Young's Modulus	Concrete	8.7 kN/mm²
	D13	174 kN/mm²
	D6	171 kN/mm²
Axial force		72 kN

2.2 Bond-Slip Characteristics

Naganumas' model[2] was used for defining the bond stress-slip characteristics between rebar and concrete. Two models were considered for peak bond strength. In model 1 peak bond strength in the beam and the column sections were calculated according to the Japanese Design guidelines[3] (shown in Eq. 1). For model 2,

simple pullout test was performed on pre-installed rebar in concrete blocks with variable embedment length[4]. The peak bond strength value found from that test was considered for the model.

$$\tau_u = 0.7\left(1 + \frac{\sigma_0}{\sigma_B}\right)\sigma_B^{2/3} \tag{1}$$

where, τ_u is bond strength; σ_0 is axial stress of column; σ_B is the compressive strength of concrete.

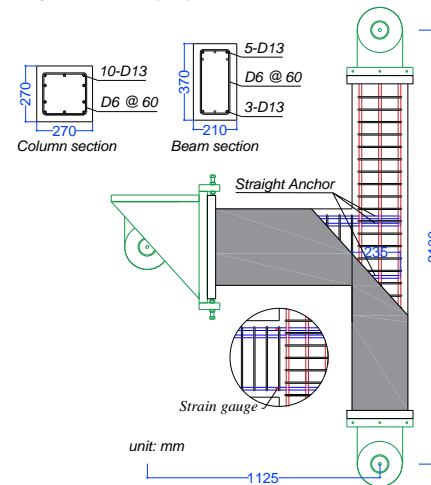Bond slip corresponding to the bond strength was assumed as 1.0 mm, referring to the study by Elmorsi et al.[5].
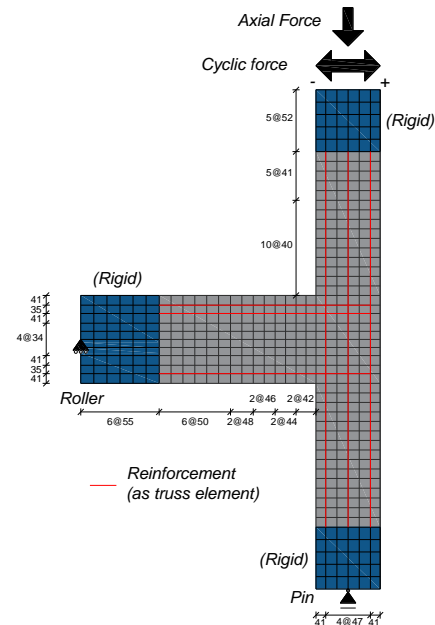

Figure 1 specimen J1 details

Figure 2 FEM element division and boundary conditions

3. Results and Discussion

Experimental results[1] in **Fig. 3** showed that specimen J1 suffered pullout at -2% drift ratio in negative loading direction. However, on the positive loading direction joint shear failure was observed.
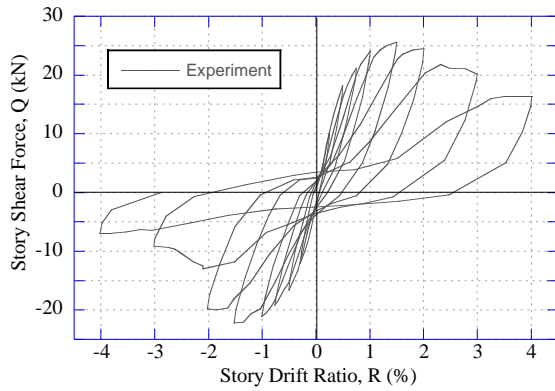
Figure 3 Experimental results[1]

The story shear force vs. story drift angle relationships from the FE analysis and experimental study are compared in **Fig. 4**. Model 1 reached a maximum strength of +25.5 kN & -19.0 kN in the positive and negative directions, respectively. Whereas for the case of model 2 it was +27.6 kN and -21.5 kN, respectively. A large slip/pullout was observed in both positive and negative loading directions for model 1. In the positive loading direction beam rebars slipped at R = +2.0% drift cycle. While, in the negative loading direction beam rebars slipped at R = -1.5%, as shown in **Fig. 5**. No rebars yielded in the FEM analysis and strains observed in the corresponding cycles were lower than those of the experiment. On the other hand, pullout was not observed in either loading direction for model 2. Rebars yielded both in positive and negative direction at 1.5% drift ratio, as shown in **Fig. 5**.
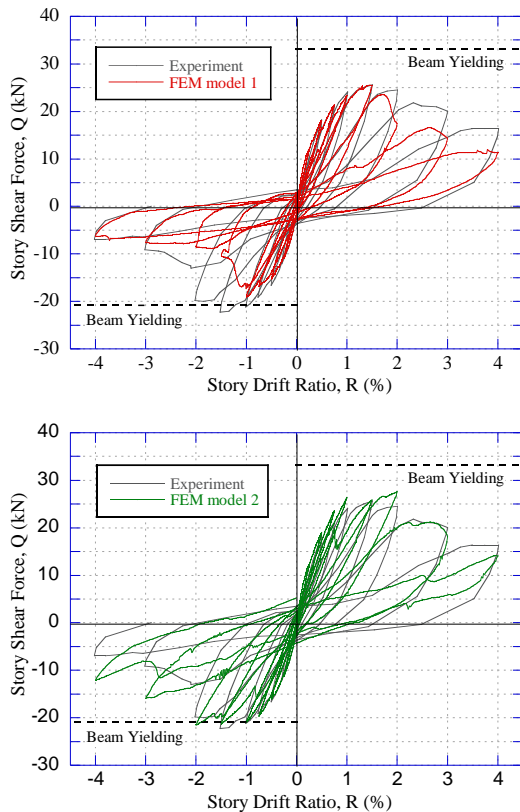

Figure 4 Story shear vs. story drift ratio relationships

For model 1 the FE analysis was successful in predicting the pullout failure mode in the negative loading direction. Furthermore, the FE analysis also showed pullout in the positive loading

direction, which was not observed during the experiment[1]. The bond strength applied to the analysis for model 1 followed the Japanese Design guidelines[3], which might be conservative compared to that in the experimental specimen. The bond strength applied to the analysis for model 2 is from pure pullout test, which might be radical compared to that in the experimental specimen.
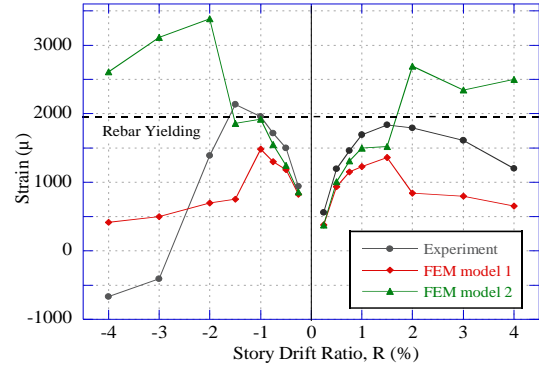

Figure 5 Beam-column joint end rebar strains

Figure 6 shows the damage to the specimen of model 1 at R= -1.5% drift ratio when pullout was observed along with the damage of the experimental specimen J1.
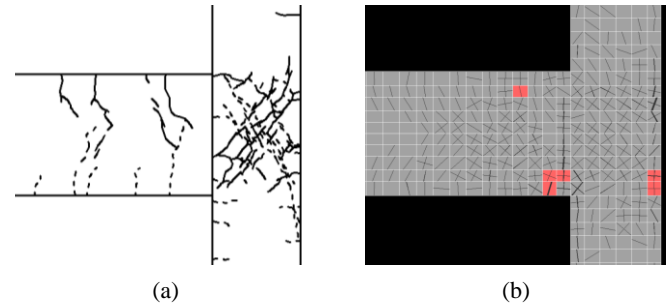

| (a) | (b) |

Figure 6 Damage at R= -1.5%; (a) experiment, (b) FE analysis

4. Conclusions

The following findings were obtained from this study:

1. Finite Element analysis showed pullout failure of beam longitudinal rebar with straight anchorage can be simulated by considering bond behavior between reinforcing bar and concrete.
2. Model 1 underestimated the joint capacity when compared to the experiment because the peak bond strength used was from design guideline, which provides conservative estimations.
3. Model 2 overestimated the joint capacity when compared to the experiment because the peak bond strength used was from element test. In real condition, the joint is damaged and the acting bond strength is lower than the simple element test.
4. To get a better estimation of the joint characteristics, bond strength needs to be determined form the sub-assembly test.

References

1) Wardi, S., Saha, N., Sanada, Y., and Takahashi, S. (2018), Proceedings of AIJ Annual Convention 2018, Paper No. 23334.
2) Naganuma, K., Yonezawa, K., Kurimoto, O. and Eto, H.;, 13th WCEE, Paper No.586, August., 2004.
3) Architectural Institute of Japan: Design Guidelines for Earthquake Resistant Reinforced Concrete Buildings Based on Inelastic Displacement Concept (Draft) 1997.
4) Saha, N., Master Thesis, Osaka University, 2019.
5) Elmorsi M, Kianoush MR, and Tso WK., Can. J. of Civil Eng. 2000; 27: 490–50

Flood Coping Mechanisms in In-city Resettlement Areas: A Case Study of Barangay Malanday in Marikina City, Philippines

Nikko Torres Ner

Architectural and Urban Planning Lab, Department of Architectural Engineering

Key Words: *in-city resettlement, coping mechanisms, urban flooding, vulnerability, disaster risk management*

1. Introduction

A World Wide Fund for Nature (WWF) study in 2009 rated Metro Manila as the most at risk among 11 mega-cities due to its exposure to typhoons and flooding (Shaw 2010). This problem is compounded by rapid urbanization and decades of unplanned development which had pushed the marginalized sector to live in blighted and high-risk areas in Metro Manila.

A 2017 study found that in-city resettlement was more efficient in the use of government resources in addressing the housing challenges in the long term compared to off-city resettlement (Ballesteros 2017). Marikina City has been implementing an in-city resettlement program since 1992. The study area, Barangay Malanday, is one of the six relocation areas for Marikina City's in-city resettlement program (See Fig. 1). The program was initiated with the motivation of revitalizing the Marikina River and relocating informal settlers away from identified danger zones at the time (Iglesias 2008).

This study intends to examine Barangay Malanday, an in-city resettlement area at risk from the effects of urban flooding, and investigate its flood vulnerability and coping mechanisms to build on existing qualitative studies that assess local knowledge and best practices towards safer cities.
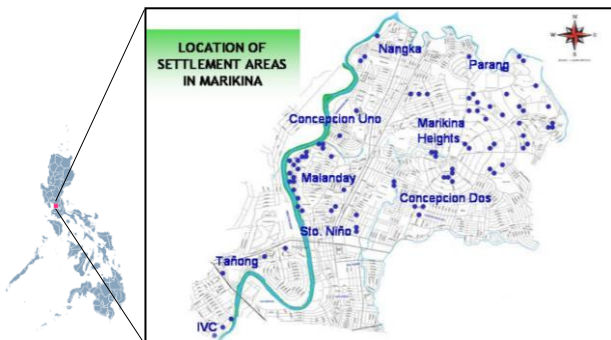

Fig. 1 In-city resettlement area locations (Iglesias 2008)

2. Research Design

2.1 Framework of Analysis

The investigation into the study area's vulnerability and coping mechanisms was guided by the Intergovernmental Panel on Climate Change's (IPCC) framework of vulnerability:

Vulnerability= (Exposure + Sensitivity)-Adaptive Capacity

- Exposure is the nature and degree to which a system is exposed to significant climate variations.
- Sensitivity is the degree to which a system is affected by climate variability.
- Adaptive Capacity is the ability to adjust to climate change to moderate potential damages

2.2 Methodology

A survey which covered 50 residents was conducted in March 2020 to gather data about respondents' area's socioeconomic profile and investigate the various flood coping mechanisms practiced by the residents. Since the area experiences flooding frequently, questions were limited to experiences pertaining to the 2009 and 2018 floods. Additional key informant interviews were conducted with homeowners' association leaders about their community's experiences in the 2009 and 2018 floods. Through semi-structured interviews, insights into their coping strategies as a community were recorded and transcribed.

Map analysis was used to gain a better understanding of the study area's level of exposure to flooding. Mapping activities were also performed to observe the effects of the respondents' coping strategies on the damage to their real and personal properties.

3. Results and Discussion

3.1 Exposure

3.1.1 Flood Hazard

The study area is situated in low-lying elevation (8-12 masl) and is in close proximity to the Marikina river. As a result, it is highly susceptible to riverine flooding caused by heavy rainfall especially in the monsoon season (June to August). The entirety of the study area falls under the very high flood susceptibility category, or areas likely to experience flood heights of greater than two meters as seen in Figure 2.
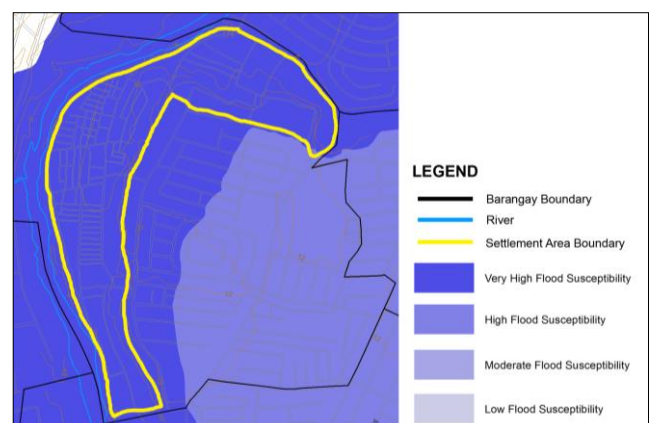

Fig. 2 Flood hazard map of the study area

3.1.2 Climate Change Projections

Models project an average temperature increase of 1.8 to 2.1 Degrees Celsius in 2050 (PAGASA 2011). With this projected temperature increase, it is expected that storms will also increase in intensity and cause more deleterious effects on the most

vulnerable populations. The amount of rainfall in Marikina City during the monsoon season (June to August) is also expected to increase by 21.3% (PAGASA 2011) from 1971-2000 levels and will increase the probability of intense flooding in the study area in the future.

3.2 Sensitivity

Three economic classes in the study area were identified from the survey, namely: poor, low-income, and lower middle class. Majority of the households fall under the poor category with 23 respondents saying they have a monthly household income of less than Php10,000 followed by low-income (17) and lower middle class (10) (See Table 1). The classification is based on criteria set by the Philippine Institute for Development Studies (PIDS) which looks at per capita income to assess standard of living.

Majority (46%) of the respondents said their household size was composed of 4-6 persons. This is consistent with the average household size in Marikina City which is 4.59 in 2019.

Table 1 Socio-economic profile (N=50)

Household Size	Count	%
1-3	9	18
4-6	23	46
7-9	14	28
<10	4	8
Monthly Household Income (PhP)	**Count**	**%**
Poor (>10,000)	23	46
Low-income (10,001-20,000)	17	34
Lower Middle Class (20,001-40,000)	10	20

3.3 Adaptive Capacity

3.3.1 Housing Modifications

Respondents were asked what modifications, if any, had they done to their houses to protect against flooding following the 2009 flood. They were then asked to rate and describe the degree of damage to their houses during the 2009 flood and then the 2018 flood. Three types of housing modification were observed, namely: building upper floors, rebuilding/reinforcing the house with more durable materials, raising/strengthening of ground floor. Figures 3 and 4 show the degree of damage to real property to the flood in 2009 compared to the flood in 2018.
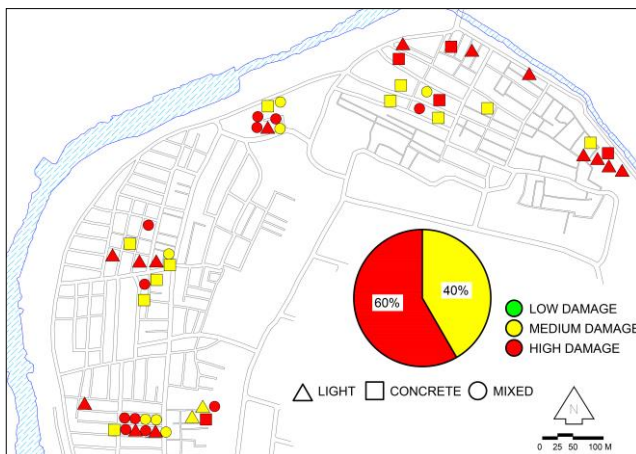

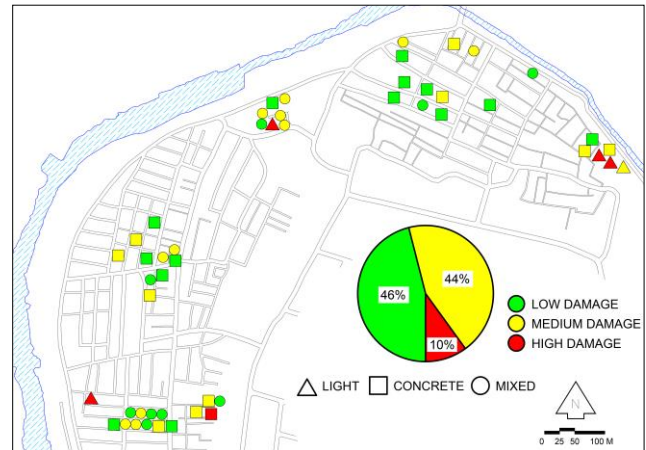Fig. 3 Degree of damage to real property in 2009 flood

Fig. 4 Degree of damage to real property in 2018 flood

3.3.2 Behavioral Changes and Preparedness

All respondents mentioned proactively heeding early warning systems and evacuation measures since 2009. In the 2009 flood, 48 (96%) of the respondents reported suffering high damage to their personal property because of complacency and ignoring the evacuation warnings. This heightened alertness from the residents during the 2018 floods translated to only 4 of the 50 respondents suffering high damage to their personal properties (See Table 2).

Homeowner's association leaders also reported that aside from their original function as facilitators of the mortgage program, they have taken on new roles such as organizing disaster training workshops and assigning specific responsibilities to their officers in times of disasters.

Table 2 Damage to personal property in 2009 vs 2018 (N=50)

Degree of Damage	2009 Flood	2018 Flood
Low	0	31
Medium	2	15
High	48	4

4.   Conclusion

Significant reduction on the impact of floods on the study area was observed in the comparison of the aftermaths of the 2009 and the 2018 floods. Reduction in damage to personal property saw the most positive improvement. This can be attributed to the disaster preparedness of individual households and their community's disaster risk management initiatives. Reduction in damage to real property, however, could still see some areas for improvement. Due to their economic situation, majority of the households can only afford incremental and low-quality improvements to their houses. A multisectoral approach which considers the residents' realities and experiences could prove to be beneficial in uplifting their current situation.

References

1) Shaw, R.: CDRI (Kyoto, Japan), pp. 3-4, 2010.
2) Ballesteros, M.: Evaluating the Benefits and Costs of Resettlement Projects-A Case Study in the Philippines, IDEAS (Exeter, United Kingdom), pp.257-271, 2017.
3) Iglesias, G.R: ADPC (Bangkok, Thailand), pp.5-7, 2008.
4) McCarthy, J. et al.: IPCC (Cambridge, UK), pp. 21-22, 2001.
5) PAGASA: Climate Change in the Philippines, PAGASA (Quezon City, Philippines), p.35, 2011.

A Study on the Potentials of Green Blue Infrastructure (GBI) Network for Dhaka City in Bangladesh

Tahmina Rahman

Laboratory of Urban planning and Design (Lab. 3),
Department of Architectural Engineering

Key Words: *Green-Blue Infrastructure, ecological services, neighborhood planning, Dhaka*

1. Introduction

Cities currently possess the highest proportion of the world's population, with an estimated 54% of the global populationt[1]. With this rapid growth of the urban population, the regeneration and conservation of urban ecosystems are becoming a serious challenge, especially in developing countries. In view of the current pace of urbanization, per capita urban green spaces have reduced tremendously in the cities, especially in the Global South. However, Green-Blue Infrastructure (GBI), as key components of the urban ecology, can play a vital role in providing the ecosystem services. The city of Dhaka has also seen its green and blue areas gradually encroached upon and destroyed[2], a situation which has steadily deteriorated since Bangladesh gained independence. In Dhaka, both public and private sectors are continuously developing natural lands within and on the outskirts of the city, without considering the environmental impact of this activity by filling the water bodies or graving the greens[4].

This study, therefore, sought to analyze the potential of GBI for the urban ecological conservation and regeneration of Dhaka city from both a macro and micro level perspective. At the macro level, spatiotemporal changes in green and blue infrastructures to propose a scheme for the protection and regeneration of the existing green spaces and water bodies is analyzed. For micro-level user's preference to determine possible options to the adoption of new GBI in dense urban neighborhoods through a design exercise for sustainability, connectivity, and well-being is assessed.

2. Methodology

2.1 Methods

This research adopted the case study strategy. In this study, multiple data from different sources (Historical maps, Policy regarding city development, Surveyed data etc.) are collected to triangulate the validity of the available information to develop an in-depth understanding on the possibilities to develop a Green Blue Infrastructure (GBI) Network for Dhaka City. The study was conducted in two phases: macro-level study and micro-level study. For the macro-level study, data was gathered through historical map regression, policy content analysis and key informant interviews. For the macro-level study, data was collected through a structured questionnaire survey of 115 samples, transect walks and field observations and photographic documentation. The fieldwork was conducted during August and September of 2019. SPSS version 23 and Microsoft Excel were used to analyze the questionnaire survey data.

2.2 Context

The study was undertaken in Dhaka city, the capital of Bangladesh. Two neighborhoods were selected based on physical morphology (street pattern, planning organizations etc.), availability of GBI and historical evidence of GBI integration.

Fig. 1 Dhaka Metropolitan Area and Studied Areas

Site A is a well-organized planned residential area with a grid-iron street pattern (Ward 49) with several GBI options such as lake, lakeside park, playgrounds of different scales, road verges, road islands and roadside green areas. Site B is an organically developed residential area with a spontaneously growing street pattern (Ward 40 (partial) and Ward 51) with several GBI options such as ponds, park, playgrounds of different scales, road verges, road islands and roadside green areas.

3. Results

3.1 Changes in Urban Green and Blue Spaces (Macro Level)

From the historical map regression, historical dynamics of urban waters and green spaces and traces in the connectivity of urban waters `were analyzed.

From the analysis, a 'large positive linear association' was found between the total area of Dhaka city and total built area from 1924 to 2015 with correlation value r= 0.966 and R^2= 0.934. However, between the total area of Dhaka city and urban greens, the association was 'small positive linear association' with the correlation value r= 0.723 and R-squared= 0.525. and similar 'small positive linear association' was also found between the total area of Dhaka city and urban waters with the correlation value r= 0.811 and R-squared= 0.658. Additionally, it was identified that the trendline of the built area has a steep incremental growth (Fig. 2). However, in the case of the urban greens and urban water, a dramatic drop was observed after 1995. Between 1960 to 1995, the proportion of the area of urban waters was steady, but also started a sharp decline after 1995. Before independence, the GBI area ratio with the built area was 51:49, persisting until 1995. However, after 1995, this dramatic fall continued and by 2015, the loss was about 25% (from 10916 ha to 8328 ha). Currently, the stock of GBI is only 27% (around 8328

ha), including restricted green and privately-owned informal greens, mostly inaccessible to the general public.
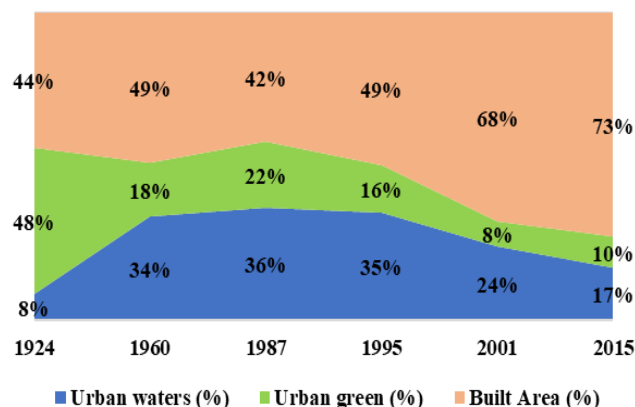

Fig. 2 Dhaka Metropolitan Area and Studied Areas

Moreover, building on the identified geomorphology and spatiotemporal changes from this research and comparing with the streamlines and water flow direction of Dhaka from the previous studies[5,6], seven potential locations where the new connections can be developed or the existing water network can be resurfaced were identified.

3.2 Availability of Urban and Green Spaces (Micro Level)

From the comparison of two studied areas (Fig. 3), it is evident that Site B, is denser in terms of built area (93.3%) and below the standard regarding the availability of GBI, (available GBI is 6.7%, only around 10 ha). On the other hand, Site A has 27.8% of greens spaces and urban waters (around 104 ha, which is about double of the maximum required open space of 57 ha, as per Open Space Standards by Detailed Area Plan, Dhaka (2010)). Therefore, Site B selected this area to demonstrate the design proposal.

Fig. 3 Surveyed Study Areas with Their GBI Options

Results from users of GBI found that the majority of the respondents (70%) lived in apartments and 60% of the total respondents used GBI for different activities. Among these activities, physical exercise and social gathering were found to be primary activities. Close proximity, multi-functionality and well-equipped space were the main attributes of their preference. 'General maintenance—littering, garbage and waste dumping' in the GBI sites was the main problem experienced by the majority (62%). Along with this, 59% of them in Site B, indicate the problem of accessibility (either no GBI in close proximity or nearby GBI has restricted Access). Last of all, their perception of the benefits of having GBI in the neighborhood has been investigated through a five-point Likert scale. A positive perception regarding the benefits of GBI has been observed except social benefits; 71% responded positively for environmental benefits, 59% responded positively for economic benefits, 60% responded positively for wellness benefits and 48% responded positively for social benefits.

4. Design Proposal

In the design exercise, a projected design development has been proposed (Fig. 4), considering Dhaka Metropolitan Building Construction Act (2008); the rules of FAR, Mandatory Open Space, Maximum Ground Coverage has been applied to demonstrate how to preserve the existing GBI and introduce interconnected green-blue spaces.

Fig. 4 Proposed Plan for Neighborhood X (NX)

5. Recommendation and Conclusion

In summary, the study showed that there has been a huge decline in blue and green spaces in Dhaka, particularly since 1995. However, the majority of the surveyed residents reported immense environmental, economic and wellness benefits to the adoption of GBI in their neighborhood. Therefore, in addition to the design proposal, the study recommends the integration of conservation and revitalization of GBI in the urban design and planning policy of Dhaka city.

References
1) Goldenberg, R., Kalantari, Z. & Destouni, G: J of LDD, Vol.29, pp. 3607-3616, 2018.
2) Chowdhury, A. & Faruqui, S.: Physical Growth of Dhaka city. Dhaka: Past, Present and Future, pp. 43-61, 1989.
3) Byomkesh, T., Nakagoshi, N. & Dewan, A. M. J of LEE, Vol.8, pp. 45-58, 2012.
4) Islam, N. Dhaka Now: Contemporary Urban Development, Dhaka, Bangladesh, Bangladesh Geographical Society, 2005.
5) Mandal, D., MT, West Virginia University, 2019.
6) Peeters, S. & Shannon, K.: Nakhara—J of EDP, Vol.7, pp. 25-46, 2011.

Impacts of Tsunami Driven Debris on Onshore Coastal Structures

N. R. Josiah

Coastal Engineering Laboratory, Department of Civil Engineering

Keywords: *Tsunami, wave, debris, impact force*

1. Introduction

Extreme coastal disasters like tsunami always bring great devastation to the properties and lives as witnessed in recent past especially during 2004 Indian Ocean tsunami and 2011 Great East Japan tsunami. Post field surveys of tsunami damages indicated that in addition to wave induced forces, floating objects (i.e. debris) carried by tsunami also contributed significant amount of forces which leads to either damage or failure of the structural facilities at inundated area (Murata et al., 2016). Debris can be a usually available objects in coastal and harbour areas can be ranged from boats, shipping vessels, containers, vehicles, damaged pieces of buildings and lumbers (Nistor et al., 2008). Even though few design guidelines (FEMA55, 2011; FEMA P646, 2012) have discussed a need of estimation and basic approaches to calculate debris caused impacts, a proper way to encounter this phenomena is currently under development. This study presents an experimental investigation conducted to examine the impact forces exerted by different type of debris to a typical one storey structure available in coastal area. Objective of the study is to identify the variation of impact forces in relation to wave forces, collision patterns and to diagnose governing parameters of debris-structure interaction provoked by a single debris element.

2. Methodology

2.1 Experimental facility

Wave tank facility at the Department of Civil Engineering, Osaka University was utilized to conduct the experiment. Figure 1 shows the experimental set-up prepared. Tsunami like flow was generated as suddenly lifting the gate of the reservoir to allow the bore to propagate. Water level difference between flume and reservoir (Δh) was varied to generate different wave bores.
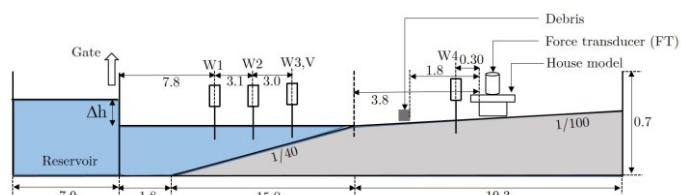

Fig.1 Sketch of the experimental set-up

A one storey house model adopted from typical house reported in Chen et al. (2005) was employed in this study. This model has a dimensions of 0.15 x 0.1 x 0.05 (length x width x height in *m*) and made up of wood.

2.2 Experiment cases

There were six contrasting flow conditions were generated to represent a band of diverse inundation depths and approaching velocities representing possible tsunami characteristics are listed in Table 1. Velocity and inundation depth were measured at the locations of *V* and *W4* as shown in Figure 1. Velocities and inundation depth in front of the house model were in the range of 0.55 *m/s* to 1.02 *m/s* and 0.033 *m* to 0.074 *m* accordingly. Properties of debris used in this study is presented in Table 2.

Table 1: Flow conditions

Case No.	Δh (*m*)	Max. velocity (*m/s*)	Max. Inundation depth (*m*)
I	0.1	0.55	0.033
II	0.12	0.63	0.046
III	0.15	0.77	0.051
IV	0.17	0.88	0.062
V	0.2	0.93	0.066
VI	0.22	1.02	0.074

Table 2: Properties of debris

No.	Type	Dimensions (*cm*)	Mass (*g*)
1		2.5x2.5x2.5	9
2		2.5x2.5x3.0	10
3		2.5x2.5x4.0	14
4		2.5x2.5x5.0	17
5	Rectangular	3.0x3.0x3.0	14
6		3.0x3.0x4.0	18
7		3.0x3.0x5.0	22
8		4.5x4.5x4.5	47
9		4.5x4.5x5.0	54
10		3	21
11	Sphere	4	47
12		5	75

3. Results and Discussion

3.1 Wave forces

Figure 2 shows the time histories of wave forces exerted on house model by each cases of wave bores listed in Table 1, without the presence of debris. Peak wave forces varied in between 0.32 *N* to 11.06 *N* due to the wave action.
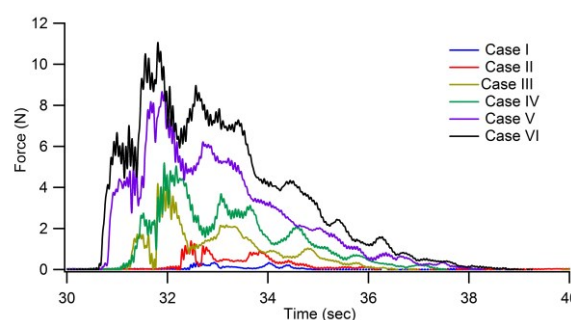

Fig.2 Wave forces on house model

3.2 Debris impacts

First, time histories of wave and debris impact forces were compared together and related maxima in each cases were identified. Figure 3 presents the shifts in maximum collision forces of rectangular debris of 2.5x2.5 cross section with the lengths of 2.5, 3, 4 and 5 *cm* varying with the maximum inundation depth measured near house model (at *W4*). Similarly, Figures 4 and 5 show the cases of rectangular debris with the cross sections of 3.0x3.0 and 4.5x4.5 respectively. Variation of peak forces for spheres are exhibited in Figure 6.
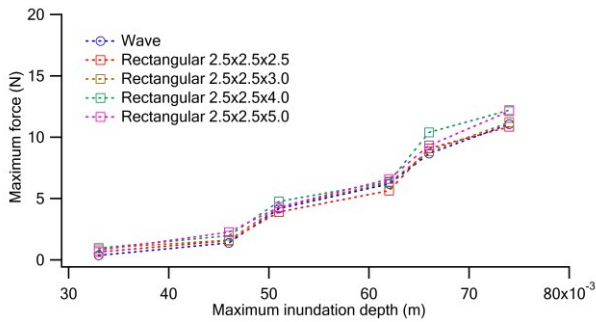
Fig.3 Maximum forces induced by rectangular 2.5x2.5
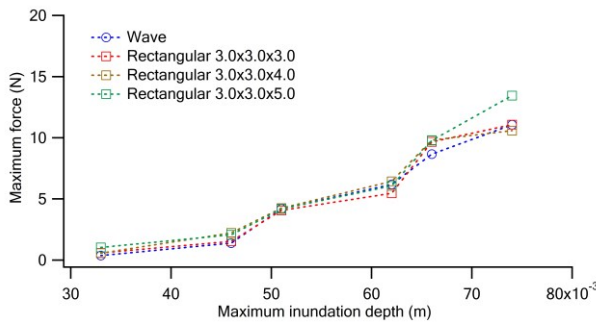
Fig.4 Maximum forces induced by rectangular 3.0x3.0
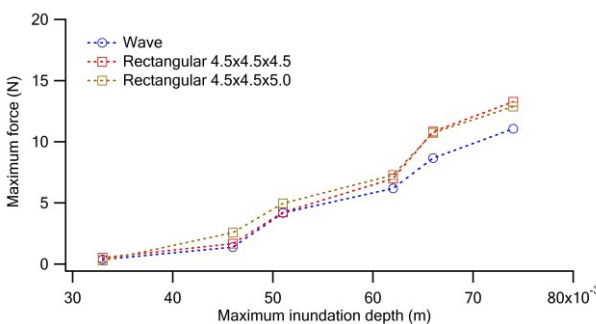

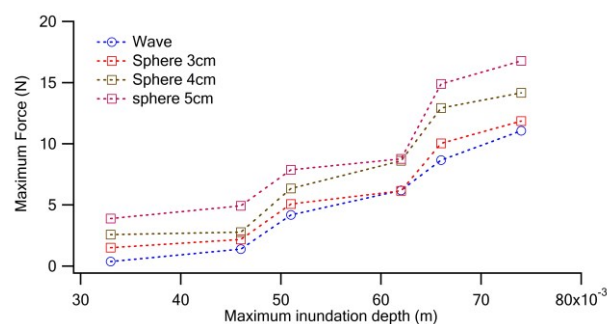Fig.5 Maximum forces induced by rectangular 4.5x4.5

Fig.6 Maximum forces induced by spheres

As detected, rectangular debris of 2.5x2.5 cross section shows a notable increment for Cases I and II and showed quite similar behavior of wave forces for other cases. For lengths of 4 *cm* and 5 *cm* of the same yielded a notably higher force than the wave effects. It might be due to the increment in size and mass of the object. Correspondingly, rectangular debris with 3.0x3.0 cross section also behaves like rectangular 2.5x2.5 debris, where objects with 3.0x3.0 cross section exerted comparably larger forces than debris 2.5x2.5. However, for the 4.5x4.5 cross section debris, the lowest flow was not able to carry the debris to the target location as wave force is dissipated in the object, thus force induced on the house also reduced. However, toward the larger flows it displayed an extensive amount of force than wave forces as the size and mass were increased. Which implies that contact area with the surface also important. On the other hand, sphere type of debris well behaved than rectangular debris as for each cases additional impact forces were significantly expanded and clearly visible than the rectangular debris. It is due to their contact area with surface is very much smaller, hence they have the ability of moving even in smaller flows. In overall, additional forces were found to be in the range of 15% to 60%. Further, initial and impacting positions of debris has a certain role in affecting the impact which was recognized for larger length rectangular debris.

4. Conclusions

This study was performed to identify the impact forces and behavior of debris brought by tsunami flow into the land area hit a typical residential facility. Rectangular and sphere type of debris with different dimensions and sizes were utilized. As observed through the experiments, debris can cause 15% to 60% of additional impact to the structures. It was noted that, smaller debris performed well in the smaller flows and for high flows their impact was not significant. For larger debris, it shows a considerable impact forces during the higher flows and during the lower flows, sometimes it was not able to move the debris in a desired way. Parameters such as inundation depth, distance between debris and house, velocity, initial and impacting positions, hydrodynamic viscosity, mass and size of debris can be considered as governing parameters.

References

1) Chen E, Ho E, Jallad N, Lam R, Lee J, Zhou Y, Re D.D, Berrios L, Nicolimo W and Ratti C (2005), Resettlement or Resilience?, The Tsunami Safer House Project, International Symposium on Disaster Reduction on Coasts Scientific Sustainable Holistic, Monash University, Australia.

2) FEMA 55 (2011), Coastal Construction Manual, 4th Edition, USA.

3) FEMA P646 (2012), Guidelines for design of structures for vertical evacuation from Tsunamis, 2nd Edition, USA.

4) Murata S, Imamura F, Katoh K, Kawata Y, Takahashi S and Takayama T (2016), Tsunami: To Survive from Tsunami, 2nd Edition, World Scientific Publications, Singapore.

5) Nistor I, Palermo D, Nouri Y, Murty T and Saatcioglu M (2008), Chapter 11, Handbook of Coastal and Ocean Engineering, World Scientific Publications.

Study on the effect of weld bead shape on fatigue strength of Out-of-Plane Gusset

BUERLIHAN AYANG

Dependability and Optimum Design, Department of Civil Engineering

Key Words: Additional weld, grinding, fatigue life, out-of-plane gusset, crack initiation and propagation

1. Introduction

With the aging of social infrastructure structures, it has become important of consideration of their maintenance. Fatigue, corrosion are the main damage factors of steel structures. The most important things in maintenance is the detection of damage such as cracks and the prediction of service life. In particular, fatigue is not limited to social infrastructure structures, but is a major factor of damage as it is said that about 80% of damage to machinery and structures is caused by fatigue. Therefore, it is important to evaluate fatigue strength correctly for properly maintain.

2. Fatigue test

2.1 Specimens

The specimens used in this experiment were out-of-plane gusset welded joints consisting of a same thickness for main plate and two gusset plates as shown in Fig. 1. The parent material for the fabrication of out-of-plane gusset was JIS G 3106 SM490YA.
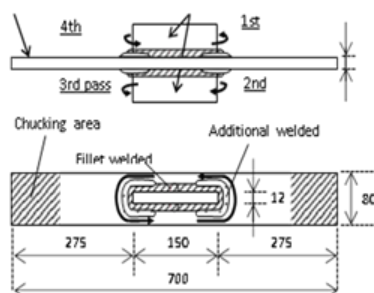

Fig.1 Geometry of specimens

The specimen used for fatigue tests divided to three types. As weld (AW), additional weld (B0, B2, B4) and the additional welding specimens treated with grinding (B0G, B2G, B4G).

2.2 Fatigue tests

Fatigue testing was performed under uniaxial tensile as the following conditions: stress ratio = 0.05, loading frequency = 7 Hz, with nominal stress ranges of 125, 150, 175, 200,225 and 250 MPa. Strain gauges were affixed to 5 mm away from each boxing weld toe on the main plate. The strain range was recorded every 5000 cycles. Crack initiation life (Nc) and Fatigue life (Nf) were defined as the numbers of cycles at which the measured strain decreased by 5% from the initial value and when the specimen fractured, respectively.

2.3 Fatigue test results and discussions

Fig. 2 shows the results fracture life. The horizontal axis of the graph indicated the number of cycles, the vertical axis shows the nominal stress range, and the average design curve of the JSSC for each fatigue class is shown by a dash line in the graph.

As it is noticed from Fig. 2, the additional welding with different weld aim position leads to improvement of fatigue strength of welded joints which is due to the noticeable increasing of weld toe radii and the significant decreasing of the flank angle. Furthermore, the more fatigue strength improvements achieve with longer weld aim position for additional weld treatment which about 1.84 times of fatigue life of AW specimen at stress range Δσ=200MPa. On the other hand, it is also shown that the fatigue strength of B2G specimens extremely extended by grinding method with about 6.89 times of AW specimen at stress range Δσ=200MPa. It is needed to be mention that the different tendency of fatigue life revealed for B0G, B2G, B4G specimens than additional weld specimens, where no more increasing of fatigue strength obtained for B4G specimen.
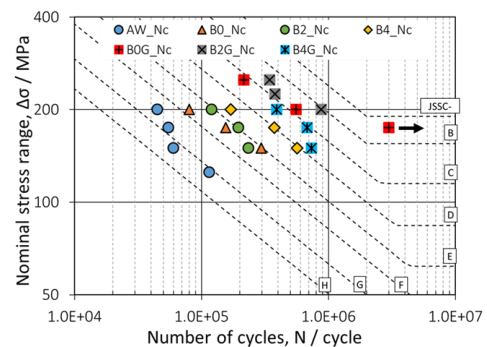

Fig.2 S-N curves for fatigue life

3. Numerical analysis for fatigue tests

3.1 FE model

3D finite element (FE) models were generated based on the specimen geometries of the fatigue test specimens by 3D scanner. The FE model and cross sections of weld bead for as weld and additional weld model were illustrated in Fig. 3. Considering the shape of the test specimens and for the purpose of the reducing of numerical costs, only 1/8 of geometry was modeled in 3D for all types of specimen.
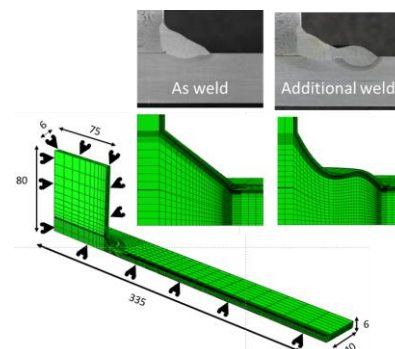

Fig. 3 FE model

3.2 Analysis conditions and assessment method

The numerical analyses were conducted in two separate steps: elastoplastic analyses and X-FEM analyses based on elastic fracture mechanics. In addition, to evaluate the effect of the shape of the additional weld bead on the stress concentration, the elastic analysis was performed.

The fatigue life of crack initiation was assessed based on the method adopted in the previous studies[1]. Fatigue S-S model[2] used for elaso-plastic analysis. The critical also was modified by considering the effect of mean stress as following equation.

$$\frac{\Delta\epsilon_t}{2} A(\sigma_m) = 0.305 N_c^{-0.580} + 0.00412 N_c^{-0.115}$$

$$A(\sigma_m) = \frac{1}{1 - 4.1 \times 10^{-4}\sigma_m - 1.6 \times 10^{-7}\sigma_m^2}$$

Where σ_m is mean stress.

Paris' law was adopted for the estimation of crack propagation fatigue life. The material constants of da/dN-ΔK average design curve were chosen based on Guidelines for Fatigue Design of Steel Structures and Explanations by JSSC[3].

3.2 Results and discussion

The Fig. 4 shows the value of Maximum principle stress for each type of model. The results revealed that the additional welding treated with grinding method remarkably reduces the stress concentration.
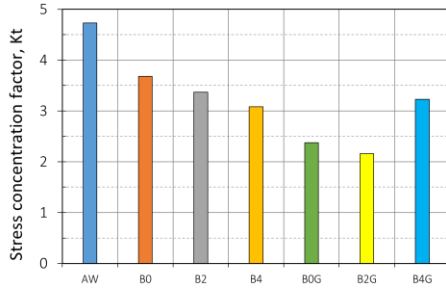
Fig. 4 The value of Maximum principle stress

Fig. 5 illustrates the S-S curves of elements with the highest cumulative plastic strain for each model at stress range Δσ = 200MPa. A smaller ratcheting is observed for B2G model compared with the AW case.
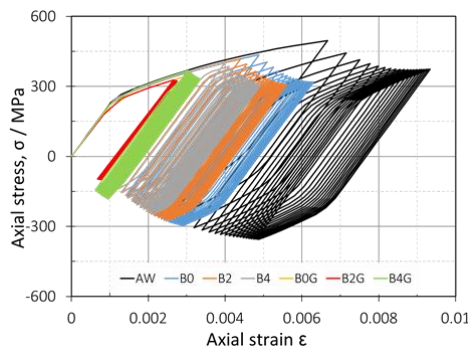
Fig. 5 4 Local stress-strain curves (Δσ = 200MPa)

From Fig. 6, it can be found that the models with an additional weld treated with grinding method models display overall a lower stress intensity factor range.
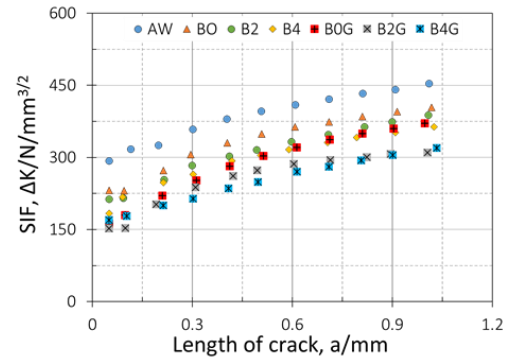
Fig. 6 SIF-a relationship (Δσ = 200MPa)

In Fig. 7, the fatigue lives obtained in the numerical simulation are compared against the experimental data for the stress range at 200 MPa. The results show that the predicted fatigue lives fairly agree with the experimental fatigue life.
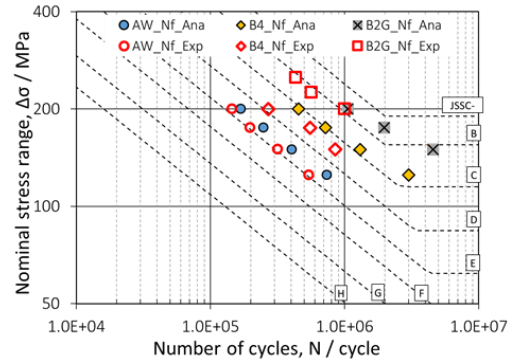
Fig. 7 S-N curve (for AW, B4, B2G cases)

4. Conclusions

1) The local stress-strain curves, evaluated at the element with the highest accumulation of plastic strain, show smallest sizes of the hysteresis loops and reduced material ratcheting in the models with additional welding treated with grinding. As a consequence, it can be concluded that this treatment is beneficial for enhancing the fatigue crack initiation life.

2) Observing the crack propagation analyses, it can be concluded that the additional welding treated with grinding method has also a small influence on crack propagation life.

3) The comparison of the numerical simulations and the experimental data revealed that the FEA can predict with a reasonable degree of agreement of the experimental fatigue life.

References

1) JSMS: Hirou Sekkei Binran, Yokendo Co.Ltd, (1995)
2) S. Tsutsumi, R. Fincato, Cyclic plasticity model for fatigue with softening behavior below macroscopic yielding, Materials & Design, 165 (2019) 107573.
3) Japanese Society of Steel Construction: Guidelines for Fatigue Design Recommendations for Steel Structures, Gihodo Shuppan, 2012.

Systematic Study of Water-on-Deck Effect of Offshore Supply Vessel Running in Stern Quartering Waves

Sreenath Subramaniam

Ship Intelligentization Subarea, Naval Architecture and Ocean Engineering

Key Words: *Water-on-deck, Systematic model runs, Shallow water deck flow, Finite volume method*

1. Introduction

Ships like offshore supply vessels and fishing vessels with an extended low weather deck could trap **water on the weather deck** when they run in high waves. This trapped water can be critical for ship transverse stability. In order to study the water-on-deck effect, a series of model experiments were conducted by Umeda, Aqmil et al. [1] in 2015 and by Umeda, Su et al. [2] in 2016. Through the experimental studies, a numerical model which considers the water-on-deck effect was developed; however, the model could not predict the actual amount of water accumulated on deck a priori, and it had to be determined by trial and error. Also, the amount of water accumulated on deck was not measured in the previous experiments.

The author took up this limitation as the research aim, i.e., to develop a numerical model which can estimate the amount of water accumulated on deck. A new set of **systematic model runs** were executed for stage-wise validation of the numerical models. New systems were added to monitor the water trapped on deck. The estimation of water-on-deck consists of two problems:

- Water inflow and outflow through openings, based on the pressure difference.
- Water flow across the deck.

For the master's course work of the author, the second problem of water flow across the deck was solved first. A numerical model based on shallow water flow theory was developed and validated against the systematic model experiment data.

2. Systematic Model Runs

2.1 Stage-Wise Planning

In order to isolate the water-on-deck effect into distinct sub-phenomenon, the systematic model runs were planned in 3-stages.

Stage 1 - General Case: At first, the author executed the most general case, which is the free-running model test with all the weather deck openings, i.e., freeing ports and stern opening opened. The results from the experiment contain the complete ship motion and water on deck phenomenon.

Stage 2 - Evaluation of ship motion: In this set of free runs, all the openings in the weather deck of the model ship were closed. Thus, the results from this set of free runs contain only the ship motion due to waves; the water-on-deck effect is not present. These results can be used to validate the ship motion part of the code.

Stage 3 - Evaluation of ship motion and water motion on deck: For this stage, all the openings in the weather deck were closed similar to the previous set of model runs; however, the deck was now filled with water in advance. Thus, the results from the experiment contain ship motion and water motion on deck, which can be used to validate the corresponding combined numerical code of ship motion and deck water flow.

2.2 Arrangement for measuring water level

For measuring the varying water level in the deck, four cameras were positioned at the four corners of the weather deck, and one camera was placed at the forecastle with a view of the deck. Scales were placed opposite to each camera placed on the weather deck to detect the changing water level. In addition, four pressure sensors were added along with the cameras. The setup is shown in Fig. 1
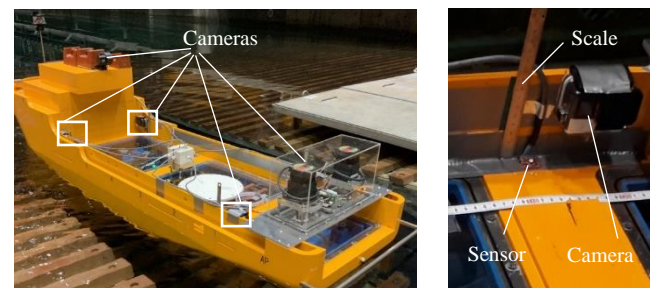

Fig. 1 Arrangement of camera and pressure sensor system

2.3 Main Observations

The author was able to confirm the presence of damping caused by the water moving across the weather deck by comparing the phase lag between ship roll motion and water motion across the weather deck, as shown in Fig. 2. The variation of damping with ship speed was also confirmed through the experiment.
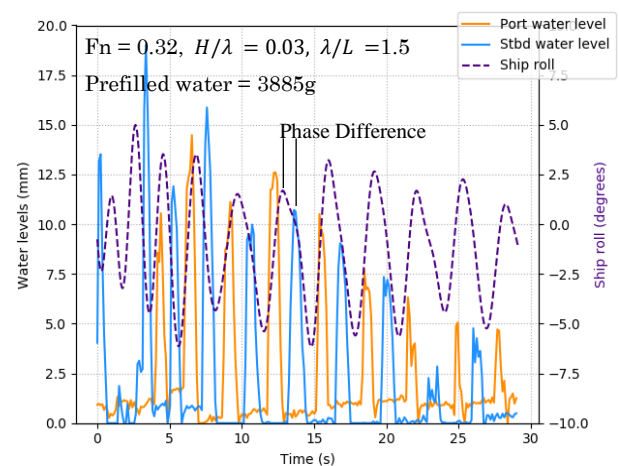

Fig. 2 Time history of ship roll and water levels

The details of the model ship, the experimental conditions and the observations were published in the proceedings of the 2020 spring conference of The Japan Society of Naval Architects and Ocean Engineers [3].

The data from Stage 3 of the model experiments were used in the validation of the deck flow model.

3. Numerical simulation of deck water flow

3.1 Coordinate system and governing equations

The body-fixed coordinate system of the ship is used to describe the motion of the fluid on the deck. When this non-inertial system undergoes motion in the space fixed inertial system, forces are induced on the fluid inside the deck.
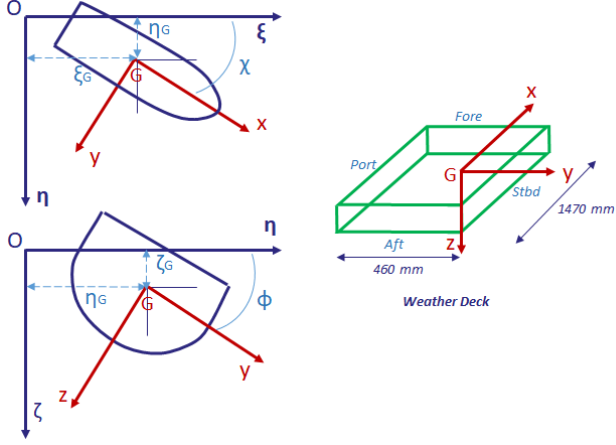

Fig. 3 Coordinate systems used to describe fluid motion

The flow of water across the weather deck is physically similar to the **shallow water flow**. In the governing equations, viscosity is neglected, and the forces due to ship motion appear as source terms in the horizontal momentum equations as shown below,

$$\frac{\partial(h)}{\partial t} + \frac{\partial(hu)}{\partial x} + \frac{\partial(hv)}{\partial y} = 0 \tag{1}$$

$$\frac{\partial(hu)}{\partial t} + \frac{\partial}{\partial x}\left(hu^2 + \frac{1}{2}gh^2\cos\theta\cos\phi\right) + \frac{\partial(huv)}{\partial y} \tag{2}$$
$$= h\left[-g\sin\theta + f_{fx} + f_{rx}\right]$$

$$\frac{\partial(hv)}{\partial t} + \frac{\partial(huv)}{\partial x} + \frac{\partial}{\partial y}\left(hv^2 + \frac{1}{2}gh^2\cos\theta\cos\phi\right) \tag{3}$$
$$= h\left[g\sin\phi\cos\theta + f_{fy} + f_{ry}\right]$$

where h is the free surface height, u is the x-component of the velocity, and v is the y-component of the velocity. $\overrightarrow{f_f}$ is the inertial force vector arising due to the ship motion. $\overrightarrow{f_r}$ is the frictional force between the deck and fluid, evaluated based on the Manning's friction slope model.[4]

The above system of hyperbolic partial differential equations is solved in the discretised deck using the **finite volume method**. [5] The structured mesh consists of 300 cells in the x-direction and 100 cells in the y-direction. Time steeping is done using the 3-step stability preserving Runge-Kutta method. The intercell numerical flux is calculated using an approximate Riemann solver and reconstruction of the solution vector at cell faces from the cell averages is carried out using forward difference together with the Van-Albada slope limiter to avoid oscillations in the final solution. Reflective wall boundary conditions are applied at the four walls of the deck and time stepping is controlled using the CFL condition to ensure stability. The Courant number is chosen as 0.9.

3.2 Results of the flow model

The deck motion is simulated in 6 DOF using the data from the gyro, and the flow of water across the deck is numerically evaluated using the developed model for deck water flow. The comparison of the water heights from simulation and experiment at the location of the aft-port side sensor is shown in Fig. 4.
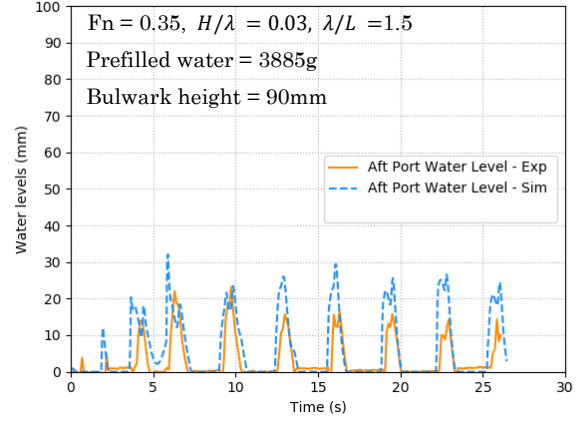

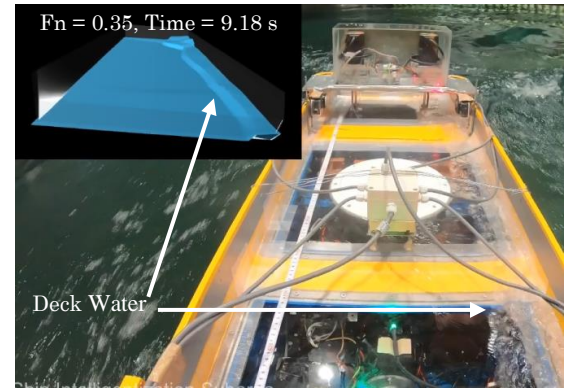Fig. 4 Comparison of water levels between exp. and sim.

Fig. 5 Deck water flow experiment vs simulation (top-left)

4. Conclusions

A new set of systematic model experiments were executed with direct measurement of the accumulated water-on-deck. The presence of damping was confirmed by comparing the phase lag between ship motion and water motion [3].

A new numerical model for deck water flow based on shallow water theory and finite volume method is developed and is successfully validated using the systematic model experiment data. This solves one of the problems involved in the numerical estimation of water-on-deck. The water ingress and egress problem will be solved in the doctoral course.

References

1) Umeda, N, Aqmil, et. al.: Proc. of 15th ISSW, pp.11-16, 2016.
2) Htun, S, Umeda, et. al.: OE, Vol. 188, Article 106225, 2019.
3) Sreenath, S, Umeda, N, Maki, A, Matsuda, A: Proc. of Spring Conference JASNAOE, pp. 623-627, 2020.
4) Tatyana, D, Alexander, K: J. Phys.: Conf. Ser. 973, 012032, 2018.
5) Fayssal, B, Mohammed, S, J of Computational and Applied Mathematics, Vol. 234, pp. 58-72, 2010.

Still Water Bending Moment Evaluation on Beam through Cargo Loading Prediction using Kalman Filter

Rodhiatul Isnaini

Ship Structural Integrity Subarea, Naval Architecture and Ocean Engineering Department

Key Words*: Kalman Filter, Cargo loading, Still Water Bending moment, Monitoring system, Inverse Problem*

1. Introduction

In general, there are two types of loads that occur in a ship. They are static and dynamic loads. A ship must be designed to be able to withstand the maximum load that is likely to be exerted on it throughout its service time. Still water bending moment (SWBM) takes up almost 1/3 of the total bending moment and is heavily influenced by the distribution of its cargo loading, which, however, has not been investigated seriously while a lot has been done on the wave bending moment. It may be attributed to a fact that the SWBM is regarded as a problem of "operation" rather than "design." It has been believed that the ship must conform to the practice of the "good seamanship".

Needless to say, for the more reasonable and rational ship design, knowing the cargo loads is crucial to predict the total hull girder vertical bending moment consisting of SWBM and wave bending moment more accurately. Additionally, by knowing the value of cargo mass, local behaviour such as double bottom bending will be able to be estimated to assure the ship safety during operation.

Recently, the structural health monitoring (SHM) using various sensors, is becoming more common. However, it does not measure the cargo loads or static loads directly and the strain measurement data often contain noise or offset drift. Sometimes it is improbable to utilize available sensors to get the desirable measurements data. This research addresses these problem by using Kalman filter and numerical model to predict the cargo loading on a beam from limited measurement data that are provided by available types of sensor in SHM, as an inverse problem. SWBM will be evaluated and compared to data that have been calculated from FEM.

2. Kalman Filter Modeling[1)]

The ship structure can be regarded as a beam that has several cargo holds. For example, in the case of cape size bulk carrier, there are nine cargo holds typically. The present problem can be reduced to a prediction of the cargo mass in each cargo hold.

Kalman filter is a recursive algorithm which works based on statistics to provides more accurate prediction of unknown variables from a system. This algorithm combines information from the system itself and a series of measurement data over time containing noise. By combining these, the covariance of predicted unknowns is able to be minimized, therefore it yields stronger and more accurate results from statistical perspective.

$$\begin{Bmatrix} x^1{}_{n+1} \\ \vdots \\ x^N{}_{n+1} \end{Bmatrix} = [F] \begin{Bmatrix} x^1{}_n \\ \vdots \\ x^N{}_n \end{Bmatrix} + \begin{Bmatrix} w^1 \\ \vdots \\ w^N \end{Bmatrix} \qquad (1)$$

$$\begin{Bmatrix} z^1{}_n \\ \vdots \\ z^M{}_n \end{Bmatrix} = [H] \begin{Bmatrix} x^1{}_n \\ \vdots \\ x^N{}_n \end{Bmatrix} + \begin{Bmatrix} v^1 \\ \vdots \\ v^N \end{Bmatrix} \qquad (2)$$

$$\{z\} = \{\varepsilon^1, \dots \varepsilon^M, \delta^1, \dots \delta^M\} \qquad (3)$$

Kalman filter consists of state-transition model and observation model that are given in equations 1 and 2, respectively. This time, cargo loading is assumed to be the state variables, and the number of predicted state variables is denoted as *N*. The observation variables, which consists of deformation and displacement data are denoted as z in equation 2 with *M* as the number of sensors. It is assumed that the deformation is measured in terms of strain. State matrix *[F]* is used to link prior and posterior state variables, while observation matrix *[H]* is used to correlate observation and state variables. The matrix may be constructed by using FE model. Moreover, this research assumes the distribution of all variables to be Gaussian with 10% white noise represented by *w* and *v*.

Strain and displacement are measured at several points on the beam. Strain was measured by using strain gauge. For both simply supported and hydro-element beams (explained later), strain gauges were placed in the same five positions. They are represented by red dots in figure 1. Meanwhile, displacement for simple beam was measured in nine points, while displacement of hydro-element beam was measured in 17 points.

The displacement data are obtained by using a motion capture system provided by an optical tracking. This system consists of high-speed tracking cameras that capture motions of an object through specific markers (grey balls in figure 1) attached to it. The whole process can be done by the help of motion capture software utilization provided by the system provider.

Table 1 Beam dimension

Type	Length	Width	Thickness
Simple beam	1000 mm	40 mm	2 mm
Hydro-element beam	1000 mm	30 mm	3 mm

3. Subject Structure

3.1 Simple Beam

The first beam that is investigated in this research is simply supported beam in air with its dimension explained further in Table 1. Experiment has been done and the output data are used to complete prediction data for Kalman filter formulation.

This time, the beam is partitioned into twelve number of elements, which represents the number of cargo holds. Moreover,

two different number of unknown variables prediction is performed. One being two number of unknown variable, and the other case assumes that there are nine numbers of unknown variable. These number of predicted unknowns represents the number of cargo holds that are estimated. Furthermore, when two cargo holds are assumed to be unknown, this means that 10 other cargo holds are assumed to be fixed. The same case is also applied for the other case. This indicates that cases in hydro-element beam analysis follow this assumption as well.

3.2 Hydro-Element Beam

The second structure is also a beam, however, floating on a water surface, (figure 1). For the modelling, a hydro-element is developed. Table 1 gives further details on its dimension. This beam is divided into 18 elements. Similar to the previous system, two types of prediction are performed. The first one is prediction with five unknown variables, while the second case assumed to be predicting nine unknown variables.

Fig.1 Hydro-element beam experiment set-up

4. Results and Discussion

4.1 Kalman Filter Implementation on Simple Beam
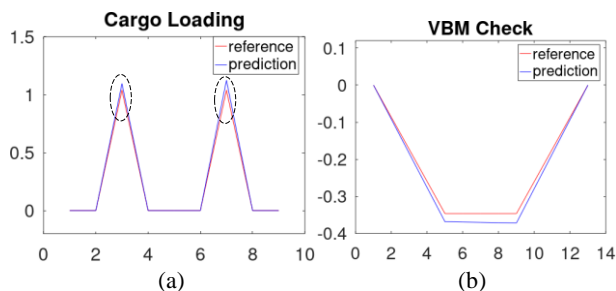

(a)   (b)

Fig. 2 (a) Two cargo loading prediction (blue) in comparison with the reference value (red) (b) Vertical bending moment obtained from prediction (blue) in comparison with its reference value (red)
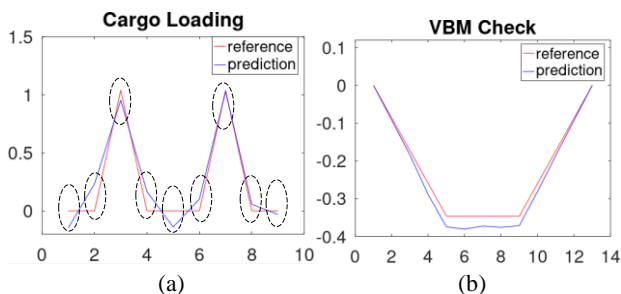

(a)   (b)

Fig. 3 (a) Nine cargo loading prediction (blue) in comparison with the reference value (red) (b) Vertical bending moment obtained from prediction (blue) in comparison with its reference value (red)

Prediction using Kalman filter based on strain and displacement data from experiment has been investigated. Figure

2 (a) shows the cargo loading prediction by assuming only two unknown variables, while figure 3 (a) presents nine unknown variables. The maximum error that is obtained from assuming two unknown variables prediction is around 8%, while the other prediction with nine unknowns has maximum error as big as 10%. As for bending moment errors, they are presented in figure 2 (b) and figure 3 (b) for two unknown predictions and nine unknown predictions, consecutively. The error that are found for bending moment values is lower than ~10% in each node, which shows that the Kalman filter works well in these predictions.

4.2 Prediction Results on Hydro-Element Beam

This subsection presents and discusses prediction results in hydro-element beam, including the bending moment results as well. Identical to section 3.2, there are two outputs of measurement data that were obtained from experiments. These data are strain and displacement that were utilized in the Kalman filter formulation.

The first case that was being evaluated is cargo loading prediction performed by assuming five unknowns. Figure 4 (a) and (b) shows cargo loading and vertical bending moment compared to its reference, consecutively. The error that have been calculated from this case are lower than 10% for both cargo loading prediction and bending moment, depicting that the filter works well for this case.
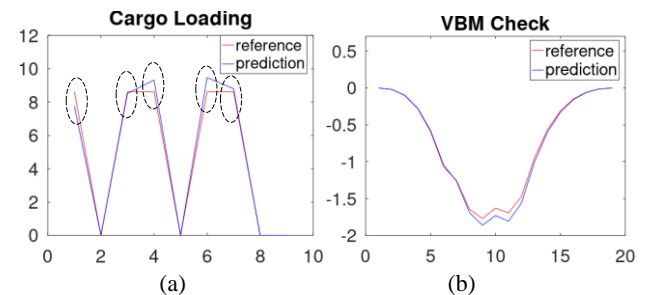

(a)   (b)

Fig. 4 (a) Five cargo loading prediction (blue) in comparison with the reference value (red) (b) Vertical bending moment obtained from prediction (blue) in comparison with its reference value (red)

The second prediction is carried out by assuming there are nine unknown variables. This arrangement, however, resulted in state variables prediction with big errors compared to its reference. This leads to high error in still water bending moment results as well. The maximum error for the bending moment result reach 50%, which is not an ideal value for error.

5. Conclusions

In this research, Kalman filter is utilized as a tool to develop a monitoring system. The system has an ability to predict cargo loading with different cases of unknown variables, as long as measurement data provides values with acceptable error.

References

1) Perisic, N. and Kirkegaard, PH.: Low-Cost Tower Root Fatigue Load Estimation for Structural Health Monitoring of Grouted Connections in Offshore Wind Turbines, Proc. Key Engineering Materials, 2013

Development of Iso-Geometric Analysis Software JWRIAN-IGA
for Weld Bead Geometry Design Using Bayesian Optimization

Thein Lin Aung

Department of Naval Architecture and Ocean Engineering

Key Words: *Isogeometric Analysis, Geometry optimization, Fillet weld bead, Bayesian*

1. Introduction

Iso-Geometric Analysis (IGA) is an emerging method of numerical simulation which uses the same data of Computer Aided Design (CAD) for both geometry description and structure analysis. In CAD geometry, B-Splines or Non-Uniform Rational B-Splines (NURBS) are commonly used to describe free-form surfaces such as the body of an automobile or the hull of a ship. On the other hand, traditional Finite Element Analysis (FEA) typically uses Lagrange polynomials to represent geometry and solution fields. Because of this difference, pre-processing such as meshing of geometry models take up much of engineering analysis time[1]. Moreover, it is difficult to feed back the analysis results to CAD environment for further design modifications. IGA is a unified method which hopes to remedy these problems by integrating CAD and FEA. This is achieved by using the same basis functions to represent the geometry and solution fields. In this way, the analysis, modelling (such as meshing by pre-processing) and evaluation (such as visualization by post-processing) become seamless and efficient, because they are working on the same platform.

In shape optimization, the parametrization of the model for the numerical evaluation of the objective function and exposing the optimization variables are of paramount importance[2]. NURBS geometries provide a convenient way to vary shape parameters since control points can directly be used and high order continuity ensures the smoothness of the boundary. Moreover, IGA enables the use of modified geometry for simulation without further pre-processing which makes the process highly automatic. In addition, the optimized geometry can be exported to CAD since the final output is also a NURBS geometry.

Bayesian optimization is a stochastic optimization method based on Bayes' Theorem in probability theory. It determines the sampling parameters by approximating the objective function from observed data by Gaussian Process. It strives to find the optimum in the fewest number of objective function evaluations as possible. Hence it is suited for applications where the function evaluation is computationally expensive such as FEA simulations.

In this study, IGA software JWRIAN-IGA is developed and the shape of a fillet weld bead under transverse load is optimized to reduce stress concentration with minimum weld volume using Bayesian Optimization.

2. Objectives

The objectives of this thesis are-
- To find the optimal shape of fillet weld using solid multi-patch IGA and Bayesian Optimization
- To study the feasibility and accuracy of IGA and Bayesian Optimization in geometry optimization problems
- To identify improvements and future research opportunities in IGA shape optimization.

3. Methodology

In Isogeometric Analysis, B-Splines or Non-Uniform Rational B-Splines (NURBS) functions are used as basis functions (shape functions) to represent both geometry and solution fields. B-Spline basis functions of order p are defined by *Cox-de Boor* recursion formula[3]:

$$N_{i,0}(\xi) = \begin{cases} 1 & , \text{if } \xi_i \leq \xi < \xi_{i+1} \\ 0 & , \text{otherwise} \end{cases} \text{ and}$$

$$N_{i,p}(\xi) = \frac{\xi - \xi_i}{\xi_{i+p} - \xi_i} N_{i,p-1}(\xi) + \frac{\xi_{i+p+1} - \xi}{\xi_{i+p+1} - \xi_{i+1}} N_{i+1,p-1}(\xi) \tag{1}$$

where ξ is the parameter value and ξ_i denotes i^{th} knot value in the knot vector $\{\xi_1, \xi_2, \dots, \xi_{(n+p+1)}\}$. A knot vector is a non-decreasing set of real numbers in the parameter space which define the mesh boundaries.

NURBS basis functions are calculated by adding an additional weight parameter w_i to each control point and taking the weighted average of B-Spline functions as shown in Eq. (2).

$$R_i^p(\xi) = \frac{N_{i,p}(\xi) w_i}{\sum_{i=1}^n N_{i,p}(\xi) \, w_i} \tag{2}$$

The symmetry model of a fillet welded T-joint is shown in Fig. 1. The geometry of fillet weld along with the base and web plates were created as separate NURBS solid patches. Second order functions were used for all patches. Each control point has 3-translational DOFs and no rotational DOF. Gaussian quadrature with full integration points was used for the integration in the domain. Multi-patch coupling is done using shared control points at patch boundaries. Linear constitutive relation is assumed with $E = 210$ GPa and $v = 0.3$ for the whole model.
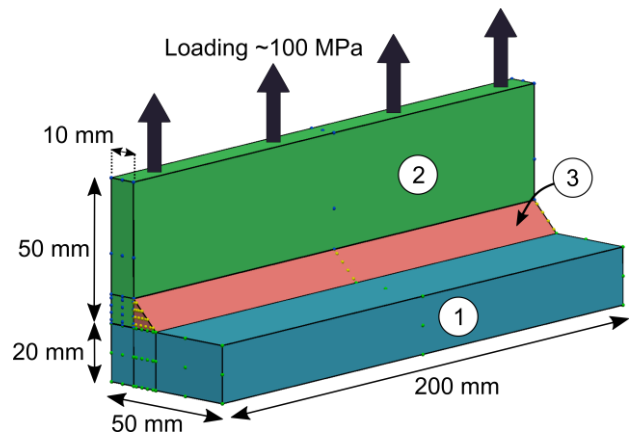

Fig. 1 Base geometry of the fillet weld model with patch numbers

The positions of control points on the top surface of fillet weld were used as variables to control the shape of the weld bead as shown in Fig. 2. After the control points were modified using the parameters from optimizer, the geometries are then refined using h-refinement (knot insertion) process to get control point mesh and knot-span mesh required for the numerical simulation. The geometry was not affected by the refinement process. The objective function was defined as a combination of maximum equivalent (Von-Mises) stress and weld volume as shown in Eq. 3.

$$\text{min: } f(\boldsymbol{d}) = \frac{max(\sigma_{eq})}{\sigma_{eq_o}} + \lambda \cdot \frac{V}{V_o} \quad (3)$$

The normalization constants were set to $\sigma_{eqo} = 100$ MPa and $V_o = 7000$ mm^3, and the penalization parameter was set to $\lambda = 1$.

The optimization variables were bounded by their respective extrema and also subject to linear constraint relations to prevent infeasible geometry configurations. The weld shape was assumed to be uniform in the longitudinal direction. The total number of optimization variables was 10 and number of iterations was 30.

Isogeometric Analysis was used as a black-box function to compute equivalent stress and weld bead volume in each geometry iteration. Newly developed in-house code JWRIAN-IGA was used for IGA and open source code BoTorch[4] was used for Bayesian Optimization.
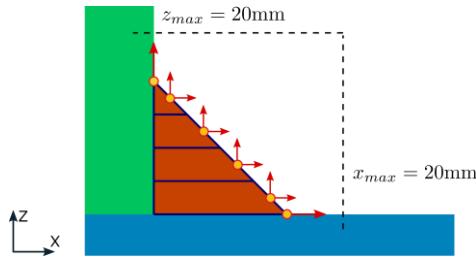

Fig. 2 Parametrization of weld geometry with optimization DOFs shown in red arrows.

4. Results and Discussion

The values of the objective function (cost) for each iteration are plotted in Fig. 3. The cost decreased significantly during the first few iterations where random parameter sets were used to fit the Gaussian model. After that, the cost generally decreased but sometimes increased in a few iterations because of the exploratory part of global optimization. In those cases, only current best value of the cost was plotted. Overall, it can be concluded that the optimization algorithm was effective since it required only 30 iterations to optimize for 10 parameters.

The shapes of weld bead for some iterations are shown in Fig. 4. The surface of the weld was a second order B-Spline curve and hence it was always smooth regardless of the discretization by control points. The numerical analysis also benefited from the exact representation of weld geometry because the shape remained exactly the same before and after mesh refinement. Generally, both the maximum equivalent stress and weld volume decreased as the iteration number increased. Each function evaluation took approximately 5 minutes and the total run time was under 3 hours by sequential iterations. This duration can be made shorter by employing parallel simulations during optimization.
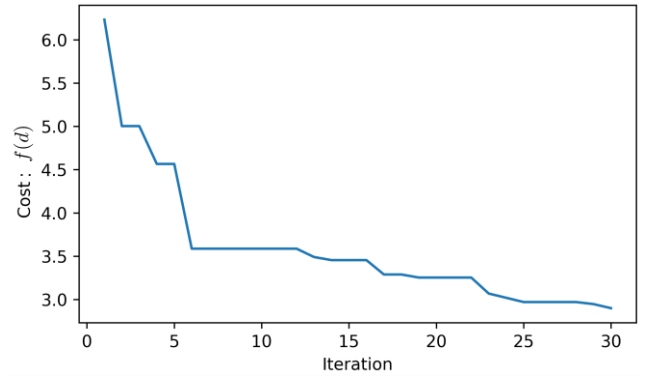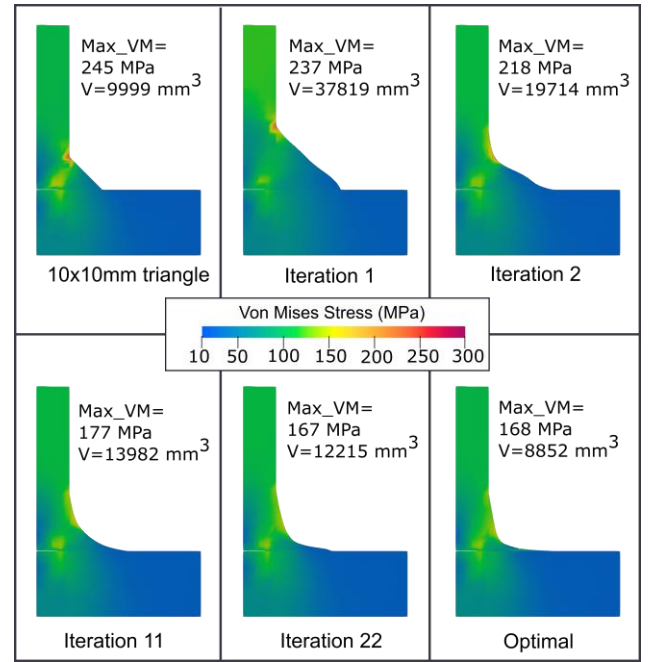

Fig. 3 Reduction of cost in each iteration step.

Fig. 4 Shapes of weld bead in selected iterations.

5. Conclusions

Isogeometric Analysis and Bayesian Optimization were used to design the optimal shape of a fillet weld to minimize stress concentration and volume of weld metal. From this study, the following conclusions can be drawn.

1. Using NURBS control points for weld shape resulted in smooth geometry parametrization
2. IGA method allowed the use of exact geometry for both optimization and analysis models
3. Bayesian Optimization achieved optimal weld shape in only 30 iterations with total run time of less than 3 hours

References

1) Hughes, T. J. R., Cottrell, J. A. & Bazilevs, Y. Isogeometric analysis: Comput. Methods Appl. Mech. Eng. 194, 4135–4195 (2005).
2) Frazier, P. I. A Tutorial on Bayesian Optimization. (2018).
3) Piegl, L. & Tiller, W. The NURBS Book. (Springer Berlin Heidelberg, 1995). doi:10.1007/978-3-642-97385-7.
4) Balandat, M. et al. BoTorch: Programmable Bayesian Optimization in PyTorch. (2019)

Study of Automatic Berthing by Evolution Strategy with Covariance Matrix Adaptation (CMA-ES) in Real Time

Dimas M. Rachman

Ship Intelligentization Subarea, Naval Architecture and Ocean Engineering Department

Key Words: *Automatic berthing, CMA-ES, Path-following, Optimal control theory*

1. Introduction

Over the past few decades, researchers have applied various mathematical strategies in designing a berthing controller. As early as 1987, Koyama et al.[1] pioneered the first systematic study about automatic berthing in which it is modeled as a linear quadratic regulator (LQR) problem where the collision risk with berth's wall is also considered. Shouji et al.[2] attempted to use nonlinear, constrained optimal control theory in the berthing controller. They modeled the berthing operation as a minimum-time problem which means, the ship shall arrive at the berthing point within the required minimum time. In solving the optimal control problem, they utilized a numerical technique called sequential conjugate gradient-restoration algorithm (SCGR).

More about optimal control problem, Maki et. al.[3] are among the first to investigate the use of CMA-ES for automatic berthing where they utilized CMA-ES to generate optimal trajectories of berthing operation along with the optimal control. They modeled the automatic berthing operation as a minimum-time problem with consideration of collision risk to the berth's wall. The study shows that CMA-ES successfully solves the nonlinear berthing problem despite the lengthy computational time. To further investigate its use in the field of naval architecture, the author attempts to employ CMA-ES in the making of an automatic berthing controller that works in real time. Since CMA-ES is a lengthy calculation, it seems not suitable to solve a difficult optimal control problem in real time like automatic berthing. However, with a few considerations in the problem definition, it is plausible to use CMA-ES in real time, which is the main scope of this thesis. Provided that [3] had established an effective means to generate optimal trajectories, the author adopts a path-following approach, where the controller will try to control the ship to follow the reference trajectories (i.e. optimal trajectories). Further, course-changing experiment is conducted to see CMA-ES performance.

2. Generation of Reference Trajectories

The optimal control problem for generating reference trajectories can be stated as follows,

Determine
$$\delta^*, n^*, t_f, t_s$$

that minimize
$$J_{ref} = \max\left(\left\|\mathbf{x}(t_f) - \mathbf{x}_{fin}(t_f)\right\|^2, \mathbf{x}_{tol}(t_f)\right)$$
$$\int_0^{t_f} \left\|\mathbf{x}(t) - \mathbf{x}_{fin}(t_f)\right\|^2 dt$$
$$+ w \sum_{i=1}^4 \int_0^{t_f} \left|\min\left[(y_{c,i} - y_{wall}), 0\right]\right| dt$$

subject to
$$\dot{\mathbf{x}}(t) = \mathbf{f}(\mathbf{x}(t), \mathbf{u}(t), t)$$
$$\mathbf{x}(0), \mathbf{x}_{fin}(t_f)$$

$$\delta(t)^2 - (\delta_{max})^2 \leq 0, \quad n(t)^2 - (n_{max})^2 \leq 0$$
$$n(t) = |n(t)| \text{ if } t \leq t_s$$
$$n(t) = -|n(t)| \text{ if } t > t_s,$$

where $\mathbf{x} = [x_0 \quad u \quad y_0 \quad v_m \quad \psi \quad r]^T$ is the state vector, and $\mathbf{u} = [\delta \quad n]^T$ is the control vector. δ^* and n^* are the optimal rudder angle and optimal propeller revolution number, respectively.

3. CMA-ES

Evolution strategy with covariance matrix adaptation (CMA-ES) is a state-of-the-art optimization technique that can guarantee global optimum at the cost of computational time. In solving the optimal control problem, CMA-ES will generate a population of the solution and calculate its mean along with the covariance matrix. After that, the samples of population are ranked based on the objective function. Those which are not feasible are eliminated. From the remaining samples, the evolution paths (direction of the next generation of population) is calculated. At the same time, covariance matrix is updated, however, with the mean from the previously generated population (both feasible and infeasible population). This covariance matrix is used to determine the step size for the next generation. Finally, a new population is generated based on the updated covariance matrix, the updated step size, and the evolution path. This process will continue until a convergence criterion is met.

4. Real Time Simulation of Automatic Berthing

CMA-ES will be used to solve a path-following optimal control problem. A path-following is a problem where the state vector at time t, or $\mathbf{x}(t)$, shall be very close to the reference state vector at the same time, or $\mathbf{x}_{ref}(t)$. However, it is more convenient numerically to discretize the problem into multiple simpler terminal-control problems, i.e., solve for the optimal control at a time $\mathbf{u}^*(t)$ that minimizes the difference between the state vector at a future time $\mathbf{x}(t + \Delta t)$ and the reference state vector at a future time $\mathbf{x}_{ref}(t + \Delta t)$.
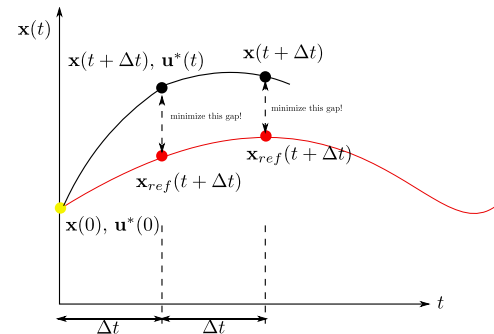

Fig. 1 Path-following terminal control problem

The objective function for this path-following problem is

$$J_{pf} = \|\mathbf{x}(t + \Delta t) - \mathbf{x}_{ref}(t + \Delta t)\|^2. \tag{1}$$

The prediction time Δt is taken as 0.8s, as this is the time that is required for the rudder of the Esso Osaka scale model ship to rotate from the maximum negative angle to the maximum positive angle.

There are six reference trajectories to be followed. It is can be seen that CMA-ES successfully controlled the ship to follow the reference trajectories under constant wind disturbance. An example is shown in Fig. 2 below. Bang-bang control (frequent switch from maximum to minimum control) happens almost for all reference trajectories. This is because we divide the problem into multiple terminal control problems which are independent to each other, so minimizing bang-bang is one of the works in progress.
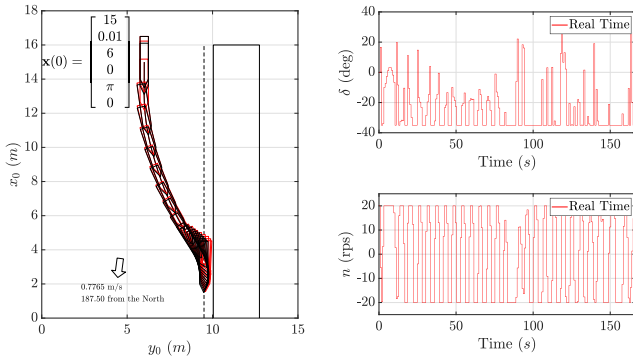

Fig. 2 Example of path-following simulation with CMA-ES, left: in red, the controlled ship; right: the controls.

However, sometimes when the trajectories are difficult to follow, CMA-ES with the objective function (1) failed to control the ship, especially for yaw and its rate. One of the ways to overcome this, is by modifying the objective function with a weight matrix $\mathbf{W} = [1 \quad 1 \quad 1 \quad 1 \quad 10 \quad 10]^T$ to cover the uncertainties and to give a sense of importance to yaw and its rate, since they are difficult to control. The weighted objective function is expressed as

$$J_{pw} = \left[\mathbf{x}(t + \Delta t) - \mathbf{x}_{ref}(t + \Delta t)\right]^T$$
$$\mathbf{W}\left[\mathbf{x}(t + \Delta t) - \mathbf{x}_{ref}(t + \Delta t)\right]. \tag{2}$$

Fig. 3 below shows CMA-ES controlled the ship to follow the reference trajectory by using the objective function shown in (2).
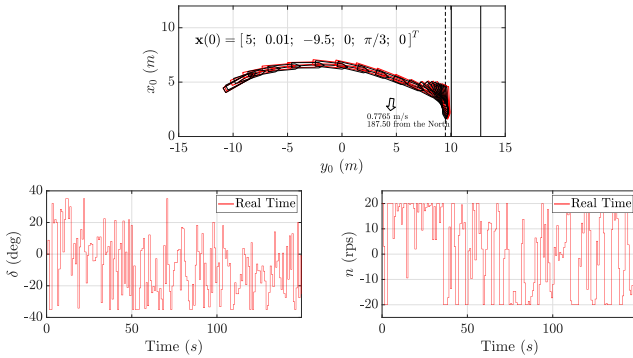

Fig. 3 Simulation with weighted objective function, upper: in red, the controlled ship; bottom: the controls.

5. Course-Changing Experiment with CMA-ES

As a first step to put CMA-ES on practice, it is utilized to control the Esso Osaka scale mode ship in a course-changing experiment. The objective function for this experiment is similar to that of a one-state path-following problem. It can be expressed as

$$J_{cc} = (\psi(t + \Delta t) - \psi_{fin})^2. \tag{3}$$

The experiment was done with a constant propeller revolution number, with three desired courses ψ_{fin} throughout the experiment (-20 from 0 s to 60 s, +20 from 60 s to 95 s, and 0 until the end). Despite the bang-bang control of rudder angle, CMA-ES proved itself worthy to control the ship in real time and in real situation at the Inukai pond without the need to execute parameter tuning like in classic PID controller.
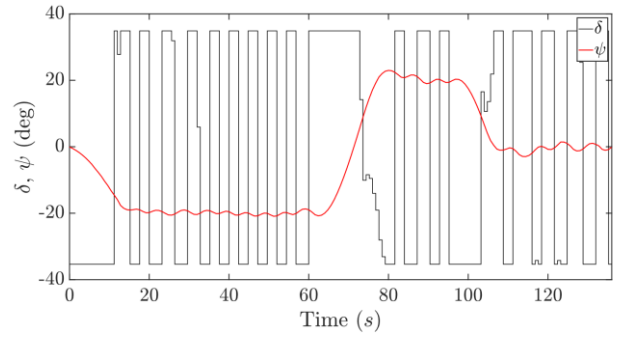

Fig. 4 Rudder angle and yaw angle in the experiment

6. Conclusion

CMA-ES is known as the state-of-the-art optimization technique but with long computational time. By simplifying the optimal control problem, the computational time can be reduced so that it can be used in real time (almost instantaneous). This has been investigated in this thesis, under constant wind disturbance, numerically. Further, as an initial step to apply CMA-ES in reality, a simple course-changing experiment was done. In this experiment, CMA-ES successfully controlled the ship to the desired courses and gave a good performance under real random external disturbances at the Inukai pond.

An important aspect is to avoid using weight matrix to create a more robust controller, i.e., no need to modify the objective function to comply with certain trajectories. One of the ways is by normalization of the state variables, which is a work on progress.

References

1) T. Koyama, J. Yan, and J. K. Huan, "A systematic study on automatic berthing control (1st report)," *Journal of the Society of Naval Architects of Japan*, vol. 1987, no. 162, pp. 201–210, 1987.

2) K. Shouji, K. Ohtsu, and S. Mizoguchi, "An automatic berthing study by optimal control techniques," *IFAC Proceedings Volumes*, vol. 25, no. 3, pp. 185–194, 1992.

3) A. Maki, N. Sakamoto, Y. Akimoto, H. Nishikawa, and N. Umeda, "Application of optimal control theory based on the evolution strategy (CMA-ES) to automatic berthing," *Journal of Marine Science and Technology*, vol. 25, no. 1, pp. 221–233, 2020.